Calcium Oscillations and Ectopic Beats in Virtual Ventricular Myocytes and Tissues: Bifurcations, Autorhythmicity and Propagation

Alan P. Benson and Arun V. Holden

Computational Biology Laboratory, School of Biomedical Sciences,
University of Leeds, Leeds LS2 9JT, UK
alan@cbiol.leeds.ac.uk
http://www.cbiol.leeds.ac.uk

Abstract. One mechanism for the onset of arrhythmias is abnormal impulse initiation such as ventricular ectopic beats. These may be caused by abnormal calcium (Ca^{2+}) cycling. The Luo-Rudy model was used to simulate the dynamics of intracellular Ca^{2+} ($[Ca^{2+}]_i$) handling and the initiation of ectopic beats in virtual ventricular myocytes and tissues. $[Ca^{2+}]_i$ in the reduced Ca^{2+} handling equations settles to a steady state at low levels of intracellular sodium ($[Na^+]_i$), but oscillates when $[Na^+]_i$ is increased. These oscillations emerge through a homoclinic bifurcation. In the whole cell, Ca^{2+} overload, brought about by inhibition of the sodium-potassium pump and elevated $[Na^+]_i$, can cause autorhythmic depolarisations. These oscillations interact with membrane currents to cause action potentials that propagate through one dimensional virtual tissue strands and two dimensional anisotropic virtual tissue sheets.

1 Introduction

Cardiac arrhythmias such as ventricular tachycardia and fibrillation are a major cause of morbidity and mortality in developed countries. Ca^{2+} overload in cardiac myocytes is well known to be a cause of delayed afterdepolarisations, where an action potential is followed by triggered activity [1, 2, 3, 4, 5]. This is a distinct arrhythmogenic mechanism from autorhythmicity, where spontaneous depolarisations occur from the resting membrane potential and do not necessarily require a preceding action potential [1]. Here we use virtual ventricular myocytes and tissues to investigate the role of Ca^{2+} in causing such autorhythmicity.

Normally, regular membrane potential (V) oscillations (the action potentials) in ventricular myocytes drive regular intracellular calcium ($[Ca^{2+}]_i$) oscillations, but under conditions of sarcoplasmic reticulum (SR) Ca^{2+} overload, Ca^{2+} is spontaneously released from the SR [3], causing $[Ca^{2+}]_i$ oscillations independently of V oscillations. These $[Ca^{2+}]_i$ oscillations can be arrhythmogenic if they interact with the cell membrane and produce transient inward currents that depolarise V past threshold. The transient inward currents that respond to spontaneous SR Ca^{2+} release could be the Na^+-Ca^{2+} exchange current I_{NaCa} and/or

A.F. Frangi et al. (Eds.): FIMH 2005, LNCS 3504, pp. 304–313, 2005.

the Ca^{2+}-activated non-specific current $I_{ns(Ca)}$ [6, 7]. Propagation of these autorhythmic depolarisations into surrounding tissue is dependent on the size of the autorhythmic focus and on the cell-cell coupling within the tissue.

One mechanism of inducing Ca^{2+} overload is block of the Na^+-K^+ pump current I_{NaK}, as seen during ischemia [8] and digitalis intoxication [9, 10] for example. The consequent build up of $[Na^+]_i$ reduces the effectiveness of the Na^+-Ca^{2+} exchanger at removing Ca^{2+} from the cell and intracellular Ca^{2+} concentrations become elevated [9].

Mathematically, the conditions that lead to this type of autorhythmicity can be identified using bifurcation analysis: at a bifurcation the qualitative behaviour of a system changes, from a single stationary solution to oscillatory activity, for example. Several previous studies have used mathematical models of atrial and Purkinje fibre cells and tissues to investigate autorhythmicity brought about by abnormal Ca^{2+} handling. Varghese & Winslow [11] examined the stability of the equations describing the Ca^{2+} subsystem in the DiFrancesco-Noble model [12] of the cardiac Purkinje fibre. Using a clamped voltage between -40 and -100 mV and constant $[Na^+]_i$ (a step justified by the slow dynamics of $[Na^+]_i$ compared to $[Ca^{2+}]_i$), they found a single stationary solution for $[Ca^{2+}]_i$ at low values of $[Na^+]_i$. As $[Na^+]_i$ was increased, a supercritical Hopf bifurcation led to an unstable fixed point and stable periodic $[Ca^{2+}]_i$ oscillations. These oscillations were shown to alter regular V oscillations in the complete model [13]. Winslow et al. [14] showed that inhibition of the Na^+-K^+ pump in an atrial cell model [15] resulted in $[Na^+]_i$ overload and $[Ca^{2+}]_i$ oscillations driving V oscillations. When a compact subset of around 1000 $[Na^+]_i$ overloaded cells were placed in the centre of a two-dimensional (2-D) tissue composed of 512 × 512 cells, the depolarisations could propagate out into the surrounding quiescent tissue. Recently, Joyner et al. [16] examined how a spontaneously depolarising focus leads to excitation of sheets of atrial and ventricular cell models, while Wilders et al. [17] examined the effects of tissue anisotropy on propagation from an autorhythmic focus in a virtual ventricular sheet.

We used the Luo-Rudy dynamic (LRd00) model of the ventricular myocyte [18] to: (i) identify bifurcations that lead to autorhythmicity; (ii) induce $[Ca^{2+}]_i$ overload and ectopic beats in single myocytes and (iii) characterise the conditions required for propagation of these beats in one dimensional (1-D) and 2-D virtual ventricular tissues.

2 Numerical Methods

LRd00 models the ventricular action potential using an ordinary differential equation (ODE) that describes the rate of change of V:

$$\frac{dV}{dt} = \frac{-1}{C_m} I_{ion} \ , \tag{1}$$

where $C_m = 1\,\mu F\,cm^{-2}$ is membrane capacitance and I_{ion} is the sum of ionic currents through the cell membrane. I_{ion} is composed of voltage gated channel

currents modelled using Hodgkin-Huxley formalism [19], as well as currents carried by other channels, pumps and exchangers. Ionic concentrations are modelled using the ODE:

$$\frac{d[\mathrm{B}]}{dt} = \frac{-I_{\mathrm{B}} \cdot A_{\mathrm{cap}}}{Vol_{\mathrm{C}} \cdot z_{\mathrm{B}} \cdot F} \ , \tag{2}$$

where [B] is the concentration of ion B, I_{B} the sum of the currents carrying ion B, A_{cap} is capacitive membrane area, Vol_{C} the volume of the compartment whose concentration is being updated, z_{B} the valency of ion B and F is the Faraday constant. Parameter values and equations describing the ionic currents can be found in [18, 20, 21, 22, 23]. Equations describing gating variables were solved using the scheme of Rush & Larsen [24], and equations of the form (1) and (2) using an explicit Euler method. The source code, written in C/C++, can be found at http://www.cwru.edu/med/CBRTC/LRdOnline/LRdModel.htm. Two variants of the model were used: one describing the Ca^{2+} handling system, the other describing a single myocyte. These were incorporated into 1-D and 2-D tissues.

2.1 Calcium Handling Equations

We reduced the LRd00 equations to those describing the Ca^{2+} handling system by applying a V clamp and using an adiabatic approximation where $[Na^+]$ and $[K^+]$ remain constant [11, 25]. V-dependent gates take on their steady-state values and, as V, $[Na^+]$ and $[K^+]$ are constant, any ionic currents that contribute only to the rate of change of these variables were removed from the system. The LRd00 equations were therefore reduced to four ODEs describing the rate of change of total $[Ca^{2+}]$ in the network SR, junctional SR, intracellular and extracellular spaces. $[Ca^{2+}]_{\mathrm{i}}$ is dependent on $[Na^+]$ via I_{NaCa} and on V via the driving force of the membrane currents and the V-dependent gates of the L-type Ca^{2+} channel (gates d and f) and the T-type Ca^{2+} channel (gates b and g). $[Na^+]_{\mathrm{i}}$ and V were therefore treated as control parameters.

2.2 Modified Single Myocyte

The complete LRd00 virtual endocardial cell was modified to induce $[Ca^{2+}]$ overload: 100% I_{NaK} inhibition, $I_{\mathrm{ns(Ca)}}$ increased twofold, $[\mathrm{CSQN}]_{\mathrm{th}}$ decreased to 7.0 mM, and the time constants of activation and inactivation of $I_{\mathrm{rel,jsrol}}$ increased to 5 ms. In all Ca^{2+} handling and single myocyte integrations, a time step of $dt = 0.01$ ms was used.

2.3 One- and Two-Dimensional Tissues

A 15 mm 1-D tissue strand composed of equal fractions of endocardial, midmyocardial and epicardial tissue [22], and a 60×60 mm 2-D anisotropic endocardial tissue sheet were used to investigate the propagation of autorhythmic depolarisations. In the 1-D tissue, the rate of change of V is given by a reaction-diffusion equation:

$$\frac{\partial V}{\partial t} = D_x \frac{\partial^2 V}{\partial x^2} - \frac{1}{C_\mathrm{m}} I_\mathrm{ion} \ , \tag{3}$$

and in the 2-D tissue:

$$\frac{\partial V}{\partial t} = D_x \frac{\partial^2 V}{\partial x^2} + D_y \frac{\partial^2 V}{\partial y^2} - \frac{1}{C_\mathrm{m}} I_\mathrm{ion} \ , \tag{4}$$

where D is a diffusion coefficient, and x and y denote directions perpendicular to and parallel to fibre axis, respectively. No-flux boundary conditions were imposed at the edges of each geometry. Ca^{2+} overloaded tissue, composed of modified LRd00 myocytes as described in Sect. 2.2, was located on the endocardial border of the 1-D strand or the centre of the 2-D sheet. Diffusion coefficients of $D_x = 0.06\,\mathrm{mm^2\,ms^{-1}}$ and $D_y = 0.1\,\mathrm{mm^2\,ms^{-1}}$ were used, giving conduction velocities for solitary plane waves of 0.4 and $0.54\,\mathrm{m\,s^{-1}}$ in the x and y directions, respectively. A time step of $dt = 0.02\,\mathrm{ms}$ and a space step of $dx = dy = 0.1\,\mathrm{mm}$ were used in both 1-D and 2-D simulations. Computation time was decreased when running 2-D simulations by tabulating the values of V-dependent exponential functions for values of V between -100 and $100\,\mathrm{mV}$ with a resolution of $0.1\,\mathrm{mV}$. Linear approximation was used for functions where V fell between the tabulated values.

3 Bifurcations in the Calcium Handling Equations

We determined behaviour of the Ca^{2+} handling equations by numerical integration over a period of 120 s, where $[Ca^{2+}]_\mathrm{i}$ either settled to a stationary stable state or oscillated. Fig. 1A is a bifurcation diagram showing stationary stable states and amplitudes of oscillations, where V is clamped at -90 mV and $[Na^+]_\mathrm{i}$ is the bifurcation parameter. The periods of the oscillations are shown in Fig. 1B. As $[Na^+]_\mathrm{i}$ is increased to $\sim$16.1 mM, large period oscillations emerge. The period of the oscillations decreases rapidly as the bifurcation parameter is further increased, indicative of a homoclinic bifurcation rather than the Hopf bifurcation identified in the DiFrancesco-Noble Purkinje fibre model by Varghese & Winslow [11]. Fig. 1C shows $[Ca^{2+}]_\mathrm{i}$ oscillations, with $V = -90$ mV, $[Na^+]_\mathrm{i} = 20\,\mathrm{mM}$ and initial Ca^{2+} concentrations as in the normal LRd00 model ($[Ca^{2+}]_\mathrm{i} = 79\,\mathrm{nM}$ at $t = 0\,\mathrm{ms}$). In this case, minimum and maximum $[Ca^{2+}]_\mathrm{i}$ is 171 and 928 nM, respectively, giving an amplitude of 757 nM and a period of 1194 ms. Fig. 1D shows the dynamics of the system in $[Na^+]_\mathrm{i}$-V parameter space for values of $[Na^+]_\mathrm{i}$ between 0 and 20 mM and for values of V between -110 and $-40\,\mathrm{mV}$.

4 Whole Cell Calcium and Voltage Oscillations

In Sect. 3 we showed that, under certain conditions, $[Ca^{2+}]_\mathrm{i}$ in LRd00 can oscillate independently of membrane potential oscillations. By unclamping the voltage, it is possible to observe whether these $[Ca^{2+}]_\mathrm{i}$ oscillations can drive transient inward currents strong enough to take the membrane potential past threshold

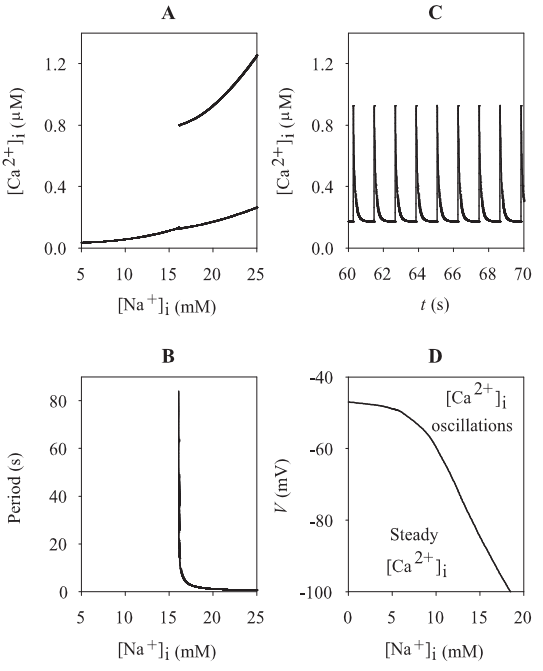

Fig. 1. Bifurcation analysis of the calcium handling equations in LRd00. **A:** Bifurcation diagram with V clamped at -90 mV, showing steady state values and oscillation amplitudes of $[Ca^{2+}]_i$. For low values of $[Na^+]_i$, $[Ca^{2+}]_i$ settles to a steady state. Oscillations emerge when $[Na^+]_i$ is increased to ∼16.1 mM. **B:** The periods of the oscillations shown in **A**. As oscillations emerge the period is large, then decreases rapidly as $[Na^+]_i$ is further increased. **C:** $[Ca^{2+}]_i$ oscillations with V clamped at -90 mV and $[Na^+]_i$ at 20 mM. **D**: $[Ca^{2+}]_i$ dynamics in $[Na^+]_i$-V parameter space. Dynamics are classified according to behaviour during the first 120 s of integration, and can either oscillate or settle to a steady state

to induce autorhythmic depolarisations. That is, we can observe whether the $[Ca^{2+}]_i$ oscillations can drive V oscillations.

$[Na^+]_i$ was clamped at 20 mM, a value that results in $[Ca^{2+}]_i$ oscillations in the Ca^{2+} handling system at LRd00 resting V of approximately -88 mV (see Fig. 1D). $[K^+]_i$ was clamped at 125 mM [11]. Integration of this modified LRd00 model revealed that $[Ca^{2+}]_i$ oscillations drive V oscillations through the action of transient inward currents. Fig. 2A shows these autorhythmic depolarisations occurring during the first 10 s of integration. The cell initially depolarises at around $t = 3.34$ s, with the action potential having an upstroke velocity of 184 mV ms^{-1}, a peak V of 28 mV and an action potential duration (APD_{90}) of 192 ms. Figs. 2B and 2C show the transient inward currents that cause V to increase past threshold. When I_{NaCa} is operating in forward mode, Ca^{2+} is extruded from the cell and Na^+ is brought in at a ratio of 1:3, and consequently the net current is inward (i.e. depolarising). $I_{ns(Ca)}$ carries both Na^+ and K^+ and so net $I_{ns(Ca)}$

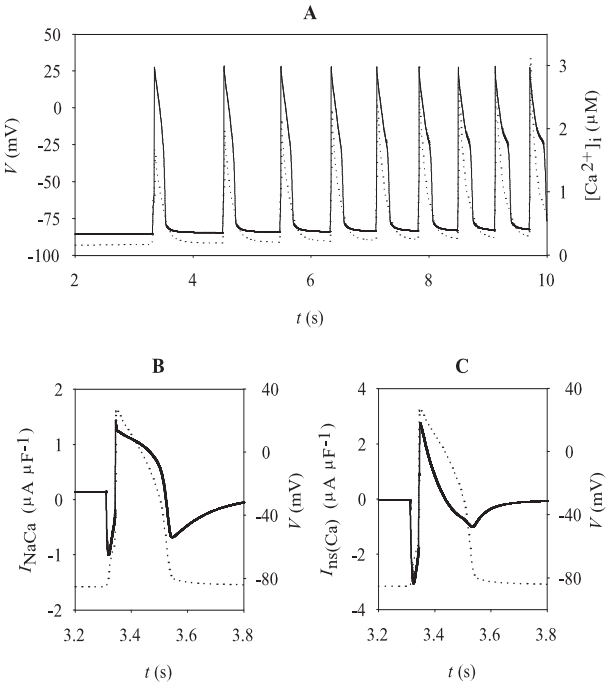

Fig. 2. Autorhythmic activity in a single modified LRd00 myocyte. **A:** $[Ca^{2+}]_i$ oscillations (dotted line) interact with the cell membrane, resulting in repetitive autorhythmic depolarisations (solid line). Both I_{NaCa} (**B**) and $I_{ns(Ca)}$ (**C**) are transiently inward, depolarising currents immediately before the depolarisation. In **B** and **C**, currents are shown as solid lines, V as dotted lines. Note that currents have been calculated for $1\,cm^2$ of membrane, and that negative current amplitudes indicate inward currents

is dependent on the sum of both these component currents. Under physiological conditions, the Na^+ current carried by $I_{ns(Ca)}$ is a depolarising inward current, while the K^+ current is a hyperpolarising outward current. Immediately before the depolarisation, both I_{NaCa} (Fig. 2B) and $I_{ns(Ca)}$ (Fig. 2C) become relatively large depolarising inward currents in response to Ca^{2+} release from the SR. This is in contrast to the other inward currents – the fast Na^+ current and the L- and T-type Ca^{2+} currents – that increase in amplitude only in response to the depolarisation (not shown). Block of either I_{NaCa} or $I_{ns(Ca)}$ causes a reduction of the membrane response to spontaneous SR Ca^{2+} release, and V remains sub-threshold: the transient inward current is only large enough to take V to threshold when both I_{NaCa} and $I_{ns(Ca)}$ are included.

5 Propagation

Propagation of an action potential from a localised area into the surrounding tissue is dependent on several factors. In 1-D and 2-D tissues, both the size of the

focus from which the action potential propagates and the cell-cell coupling within and between the autorhythmic and quiescent tissues are important. Additionally in 2-D tissues, the degree of anisotropy present and the curvature of the wavefront both affect propagation.

A minimum of 3.4 mm of Ca^{2+} overloaded tissue located on the endocardial border was required to produce repetitive propagation of action potentials through the 1-D heterogeneous tissue strand. Fig. 3A is a space-time plot showing these depolarisations emerging from the autorhythmic focus and propagating along the strand during the first 5 s of integration. The initial depolarisation propagates with a wavefront velocity of $0.4\,\mathrm{m\,s^{-1}}$, taking 28.8 ms to reach the epicardial border from the edge of the autorhythmic focus. The period of the depolarisations in the autorhythmic focus is ∼1072 ms during the first 5 s, decreasing with time presumably as ionic concentrations accumulate or deplete (due to Na^+-K^+ pump inhibition) and affect membrane conductance. As no-flux boundary conditions are used, the liminal length (the minimum amount of excited tissue located in the middle of a strand required to produce bi-directional propagation) is 6.8 mm. Here we used a spatially homogeneous diffusion coefficient of $D_x = 0.06\,\mathrm{mm^2\,ms^{-1}}$. However, alterations in cell-cell coupling (modelled as the diffusion coefficient, D), either within the autorhythmic focus, within the quiescent tissue, or at the interface of the two, will affect the behaviour of these tissues and, therefore, the liminal length required for propagation [26].

In the 2-D anisotropic endocardial tissue, repetitive propagation of autorhythmic depolarisations from a central circular focus occurred with a minimum focus radius of 5 mm, giving a liminal area of $79\,\mathrm{mm^2}$. This radius is larger than the 3.4 mm in the 1-D strand as the excitatory current provided by the autorhythmic focus must distribute over a larger area due to the curved border of the 2-D focus [27], even though increasing anisotropy has been shown to decrease the liminal area [17]. With LRd00 cell dimensions of 100×22 μm [18], the liminal area is composed of nearly 36,000 cells. This is in comparison to the liminal area of ∼1,000 cells found by Winslow et al. [14] using an atrial cell network model. Figures 3B-E show snapshots of the propagation of a single action potential through the tissue at times 910, 935, 960 and 1120 ms, respectively. As well as the direct effects of cell-cell coupling (i.e., the passive electrical properties of the tissue), the geometry of the wavefront also affects propagation [27]: the wavefront here is not a simple plane wave but is curved due to the circular autorhythmic focus, and this convex wavefront curvature acts to reduce conduction velocity. Thus the shape of the autorhythmic focus (and therefore the shape of the propagating wavefront) affects propagation. Additionally, the degree of anisotropy will affect conduction velocity through this mechanism, as the wavefront is less convex in the direction of lower cell-to-cell coupling, with this discrepancy increasing as the wave propagates (compare, for example, Figs. 3B and 3C). Both these mechanisms cause a decrease of conduction velocity; as the wavefront geometry changes with distance from the focus, wavefront conduction velocity will also change.

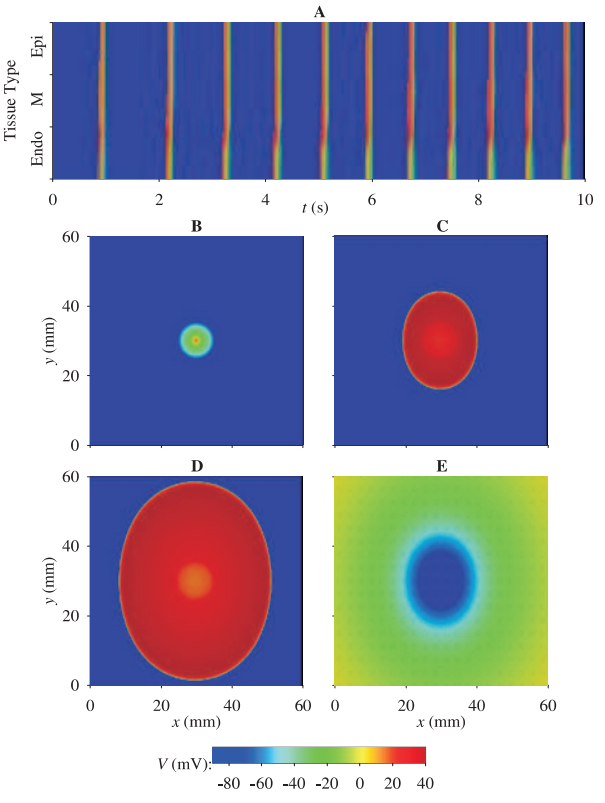

Fig. 3. Propagation of autorhythmic depolarisations in virtual tissues. **A**: Space-time plot showing propagation from a 3.4 mm autorhythmic focus located on the endocardial border of a 15 mm heterogeneous LRd00 virtual tissue strand. **B**-**E**: Snapshots showing propagation from an autorhythmic focus 5 mm in radius, located in the centre of a 60 × 60 mm 2-D anisotropic endocardial LRd00 virtual tissue sheet, at t = 910, 935, 960 and 1120 ms, respectively

6 Conclusions

We have shown that Ca^{2+} overload, brought about via inhibition of the Na^+-K^+ pump, can cause propagating autorhythmic activity in virtual ventricular myocytes and tissues of the LRd00 family. $[Ca^{2+}]_i$ in the Ca^{2+} handling equations settles to a steady state at low levels of $[Na^+]_i$, but oscillates when $[Na^+]_i$ is increased; these oscillations emerge via a homoclinic bifurcation. In the whole cell, the $[Ca^{2+}]_i$ oscillations interact with the membrane currents I_{NaCa} and $I_{ns(Ca)}$ to cause autorhythmic depolarisations that, if spatially localised, can propagate through 1-D heterogeneous virtual tissue strands and 2-D homogeneous anisotropic virtual tissue sheets. The shape of the 2-D focus and the degree of tissue anisotropy affect both the liminal area of the focus and the conduction of the wavefront through the 2-D tissue.

APB is supported by a Medical Research Council bio-informatics (computational biology) priority area research studentship (G74/63).

References

1. Wit, A.L., Rosen, M.R.: Afterdepolarizations and triggered activity: distinction from automaticity as an arrhythmogenic mechanism. In: Fozzard, H.A., Haber, E., Jennings, R.B., Katz, A.M., Morgan, H.E. (eds.): The heart and cardiovascular system: scientific foundations, 2nd ed. Raven Press, New York (1991) 2113-2163
2. Luo C.H., Rudy, Y.: A dynamic model of the cardiac action potential. II. Afterdepolarizations, triggered activity, and potentiation. Circ. Res. **74** (1994) 1097-1113
3. Bers, D.M.: Excitation-Contraction Coupling and Cardiac Contractile Force, 2nd ed. Klewer Academic Publishers, Dordrecht, The Netherlands (2001)
4. Verkerk, A.O., Veldkamp, M.W., Baartscheer, A., Schumacher, C.A., Klopping, C., van Ginneken, A.C., Ravesloot, J.H.: Ionic mechanism of delayed afterdepolarizations in ventricular cells isolated from human end-stage failing hearts. Circ. **104** (2001) 2728-2733
5. Spencer, C.I., Sham, J.S.: Effects of Na^+/Ca^{2+} exchange induced by SR Ca^{2+} release on action potentials and afterdepolarizations in guinea pig ventricular myocytes. Am. J. Physiol. **285** (2003) H2552-H2562
6. Noble, D., DiFrancesco, D., Denyer, J.: Ionic mechanisms in normal and abnormal cardiac pacemaker activity. In: Jacklet, J.W. (ed.): Neuronal and cellular oscillators. Marcel Dekker Inc, New York (1989) 59-85
7. Omichi, C., Lamp, S.T., Lin, S.-F., Yang, J., Baher, A., Zhou, S., Attin, M., Lee, M.-H., Karagueuzian, H.S., Kogan, B., Qu, Z., Garfinkel, A., Chen, P.-S., Weiss, J.N.: Intracellular Ca dynamics in ventricular fibrillation. Am. J. Physiol. **286** (2004) H1836-H1844
8. Carmeliet, E.: Cardiac ionic currents and acute ischemia: from channels to arrhythmias. Physiol. Rev. **79** (1999) 917-1017
9. Kass, R.S., Tsien, R.W., Weingart, R.: Ionic basis of transient inward current induced by strophanthidin in cardiac Purkinje fibres. J. Physiol. **281** (1978) 209-226
10. Gheorghiade, M., Adams, K.F., Colucci, W.F.: Digoxin in the management of cardiovascular disorders. Circ. **109** (2004) 2959-2964
11. Varghese, A., Winslow, R.L.: Dynamics of the calcium subsystem in cardiac Purkinje fibers. Physica D **68** (1993) 364-386
12. DiFrancesco, D., Noble, D.: A model of cardiac electrical activity incorporating ionic pumps and concentration changes. Phil. Trans. Roy. Soc. (Lond.) B **307** (1985) 353-398
13. Varghese, A., Winslow, R.L.: Dynamics of abnormal pacemaking activity in cardiac Purkinje fibers. J. Theor. Biol. **168** (1994) 407-420
14. Winslow, R.L., Varghese, A., Noble, D., Adlakha, C., Hoythya, A.: Generation and propagation of ectopic beats induced by spatially localized Na-K pump inhibition in atrial network models. Proc. Roy. Soc. (Lond.) B **254** (1993) 55-61
15. Earm, Y.E., Noble, D.: A model of the single atrial cell: relation between calcium current and calcium release. Proc. Roy. Soc. (Lond.) B **240** (1990) 83-96
16. Joyner, R.W., Wang, Y.-G., Wilders, R., Golod, D.A., Wagner, M.B., Kumar, R., Goolsby, W.N.: A spontaneously active focus drives a model atrial sheet more easily than a model ventricular sheet. Am. J. Physiol. **279** (2000) H752-H763

17. Wilders, R., Wagner, M.B., Golod, D.A., Kumar, R., Wang, Y.-G., Goolsby, W.N., Joyner, R.W., Jongsma, H.J.: Effects of anisotropy on the development of cardiac arrhythmias associated with focal activity. Pflug. Arch. **441** (2000) 301-312
18. Luo C.H., Rudy, Y.: A dynamic model of the cardiac action potential. I. Simulations of ionic currents and concentration changes. Circ. Res. **74** (1994) 1071-1096
19. Hodgkin, A.L., Huxley, A.F.: A quantitative description of membrane current and its application to conduction and excitation in nerve. J. Physiol. **117** (1952) 500-544
20. Luo C.H., Rudy, Y.: A model of the ventricular cardiac action potential: depolarization, repolarization, and their interaction. Circ. Res. **68** (1991) 1501-1526
21. Zeng, J., Laurita, K.R., Rosenbaum, D.S., Rudy, Y.: Two components of the delayed rectifier K^+ current in ventricular myocytes of the guinea pig type: theoretical formulation and their role in repolarization. Circ. Res. **77** (1995) 140-152
22. Viswanathan, P.C., Shaw, R.M., Rudy, Y.: Effects of I_{Kr} and I_{Ks} heterogeneity on action potential duration and its rate-dependence: a simulation study. Circ. **99** (1999) 2466-2474
23. Faber, G.M., Rudy, Y.: Action potential and contractility changes in $[\mathrm{Na}^+]_{\mathrm{i}}$ overloaded cardiac myocytes: a simulation study. Biophys. J. **78** (2000) 2392-2404
24. Rush, S., Larsen, H.: A practical algorithm for solving dynamic membrane equations. IEEE Trans. Biomed. Eng. **25** (1978) 389-392
25. Guckenheimer, J., Labouriau, I.S.: Bifurcation of the Hodgkin and Huxley equations: a new twist. Bull. Math. Biol. **55** (1993) 937-952
26. Benson, A.P., Holden, A.V., Kharche, S., Tong, W.C.: Endogenous driving and synchronization in cardiac and uterine virtual tissues: bifurcations and local coupling. Phil. Trans. Roy. Soc. (Lond.) A (to appear)
27. Fast, V.G., Kléber, A.G.: Role of wavefront curvature in propagation of cardiac impulse. Cardiovasc. Res. **33** (1997) 258-271